

## Two-photon retinal theranostics by adaptive compact laser source

Podlipec, R.; Mur, J.; Petelin, J.; Štrancar, J.; Petkovšek, R.;

Originally published:

May 2020

**Applied Physics A 126(2020), 405**

DOI: <https://doi.org/10.1007/s00339-020-03587-2>

Perma-Link to Publication Repository of HZDR:

<https://www.hzdr.de/publications/Publ-31086>

Release of the secondary publication  
on the basis of the German Copyright Law § 38 Section 4.

1 **Title:**

2 Towards advanced retinal theranostics by adaptive two-photon compact laser source  
3 (Two-photon retinal theranostics by adaptive compact laser source)  
4

5 **Authors: Rok Podlipec, Jaka Mur, Jaka Petelin, Janez Strancar, Rok Petkovšek\***  
6

7 **Affiliation:**

8 Rok Podlipec, Helmholtz-Zentrum Dresden-Rossendorf e.V. (HZDR), Ion Beam Center, Bautzner  
9 Landstraße 400, Dresden 01328, Germany; Jožef Stefan Institute, Jamova cesta 39, SI-1000 Ljubljana,  
10 Slovenia; email: [rok.podlipec@ijs.si](mailto:rok.podlipec@ijs.si)  
11

12 Jaka Mur, University of Ljubljana, Faculty of Mechanical Engineering, Aškerčeva 6, SI-1000 Ljubljana,  
13 Slovenia, email: [jaka.mur@fs.uni-lj.si](mailto:jaka.mur@fs.uni-lj.si)  
14

15 Jaka Petelin, University of Ljubljana, Faculty of Mechanical Engineering, Aškerčeva 6, SI-1000 Ljubljana,  
16 Slovenia, email: [jaka.petelin@fs.uni-lj.si](mailto:jaka.petelin@fs.uni-lj.si)  
17

18 Janez Strancar, Jožef Stefan Institute, Jamova cesta 39, SI-1000 Ljubljana, Slovenia; email:  
19 [janez.strancar@ijs.si](mailto:janez.strancar@ijs.si)  
20

21 Rok Petkovšek, University of Ljubljana, Faculty of Mechanical Engineering, Aškerčeva 6, SI-1000  
22 Ljubljana, Slovenia, email: [rok.petkovsek@fs.uni-lj.si](mailto:rok.petkovsek@fs.uni-lj.si)  
23

24  
25 **Abstract:**

26 To avoid a devastating effect of eye vision impairment on the information flow from the eye to our  
27 brain, enormous effort is being put during the last decades into the development of more sensitive  
28 diagnostics and more efficient therapies of retinal tissue. While morphology can be impressively  
29 imaged by Optical Coherence Tomography, molecular-associated pathology information can be  
30 provided almost exclusively by auto-fluorescence-based methods. Among the latter, the recently  
31 developed Fluorescence lifetime imaging ophthalmoscopy (FLIO) has the potential to provide both  
32 structural information and interacting pictures at the same time. The requirements for FLIO laser  
33 sources are almost orthogonal to the laser sources used in phototherapy that is expected to follow-up  
34 the FLIO diagnostics. To make theranostics more effective and cheaper, the complete system would  
35 need to couple at least the modalities of low power high repetition rate FLIO and precision high-pulse  
36 energy adjustable repetition rate phototherapy. In addition, the intermediate power high repetition  
37 rate for two-photon excitation would also be desired to increase the depth resolution. In our work,  
38 compact fiber-laser-based on high-speed gain-switched laser diode has been shown to achieve  
39 adaptable / independently tunable repetition rate and energy per pulse allowing coupled fluorescence  
40 lifetime diagnostics via two-photon excitation and phototherapy via laser-induced photodisruption on  
41 a local molecular environment in a complex ex-vivo retinal tissue.  
42

43 **Keywords:**

44 adaptable fiber laser; retinal tissue; theranostics; multimodal imaging; fluorescence lifetime imaging

## 45 1 Introduction

46 Remarkable progress in the development of advanced retinal diagnostics and therapies has been done  
47 in the last decade to provide better sensitivity and specificity for detecting retinal pathologies and to  
48 minimize the potential risks for damaging the targeted tissue.

49 Two large families of diagnostic methods evolved, the first based on detecting retinal fluorescence in  
50 the visual part of the spectrum called Fundus Autofluorescence (FAF) [1,2] and the second based on  
51 the interferometric imaging of retinal layers with NIR light called Optical Coherence Tomography (OCT)  
52 [3]. Although, OCT has been developed to an impressive (even 3D) imaging tool [4], its physical  
53 background, i.e. interference of the light differently scattered from different tissue structures, hinders  
54 more specific identification of the physiologies or pathologies particularly present in the aging retina  
55 [5]. On the contrary, FAF being sensitive to the local molecular environment [6] can provide besides  
56 morphological more indicative pathology-related information. One of the latest developments based  
57 on FAF is fluorescence lifetime imaging ophthalmoscopy (FLIO), implemented by Heidelberg  
58 Engineering [7–9], or custom FLIO systems [10,11]. The method can monitor changes in environmental  
59 parameters such as recognizing and identifying the early stages of diabetic retinopathy (DR) [8] or age-  
60 related macular degeneration (AMD) [12,13] and can provide metabolic mapping [14] unravelling  
61 various macular and retinal diseases [15]. The instrumentation relies on the sub-picosecond pulsed  
62 lasers with high repetition rates from few MHz [16] to few tens of MHz [17], encompassing typical  
63 rates of mode-locked oscillators and fast detection electronics [18] for FLIO resolution of nearly 100 ps.

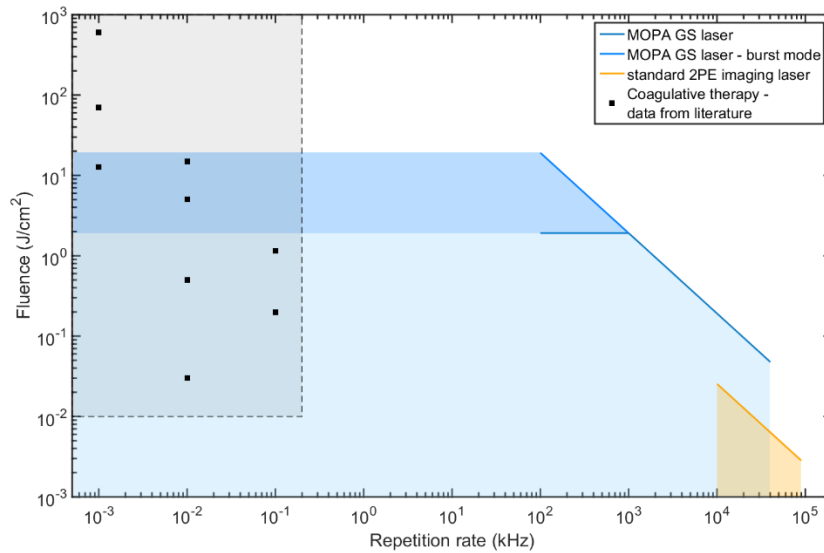
64 Current therapeutic techniques, unlike diagnostics, employ lasers with pulse duration typically orders  
65 of magnitude longer, from  $\mu\text{s}$  for Selective Retina Therapy (SRT) [19,20] to ms for Pan Retinal  
66 Photocoagulation (PRT) [21]. By low repetition rates and high energy per pulse or fluence (see the  
67 schematics in Fig. 1) they provide enough thermal effect for the therapy being effective. However, due  
68 to strong absorption on the highly absorbing retinal epithelium, the local dispersion of thermal effects  
69 is still rather poorly defined and typically widespread causing additional complications in adjacent  
70 tissue [22]. To better localize the therapeutic effect, laser pulses should in principle be faster, e.g.  
71 below  $\mu\text{s}$ , but still with enough energy per pulse to deliver efficient therapy. Thus, the technology  
72 based on nanosecond laser pulses has been recently developed with already some success in clinical  
73 trials to prevent progression of the degeneration processes in AMD [23]. Furthermore, with the  
74 development of femtosecond laser technology and its high ability to generate therapeutic effects with  
75 markedly less energy per pulse, new possibilities emerged for the modern biomedical field. A few  
76 successful clinical therapies have already been applied to corneal eye tissues, where such short pulses  
77 can produce various non-linear, photo-disruptive optical effects [24].

78 To exploit the best of the described diagnostics and therapy approaches, the great challenge in the  
79 field still lies in developing the adaptive system combining both, diagnostics and adaptive therapy at  
80 the same time and not in a sequential way. Such theranostic principle would enable more localized  
81 targeting and after-treatment-pulse diagnostics, not being possible with current systems.

82 The goal of our work was thus to overcome the current limitations of the retinal diagnostic and  
83 therapeutic laser sources and boost the development of a more universal laser source concept and its  
84 application. One direction is high power mode-locked fs laser technology (Ti:Sapphire), which was  
85 already shown promising for diagnostics with the ability to do two-photon excitation FLIO [11,15] and  
86 could as well be promising for the therapy if enough energy of high repetition pulses is accumulated.  
87 However, the lasers lack the flexibility in terms of an adjustable repetition rate to be able to increase  
88 energy per pulse needed for efficient therapy and are rather complex, making them particularly  
89 expensive.

90 To address this challenge, we herein present the design and application of the recently developed ps  
91 compact fiber laser in near-IR based on a gain switched laser diode, capable of pre-diagnostics, therapy

92 and post-diagnostics done on *ex-vivo* human retinal samples. The system enables to couple the  
 93 modalities of low pulse energy-high repetition rate (40 MHz) two-photon excitation for diagnostics  
 94 (FLIO) and high pulse energy-low repetition rate (1 kHz) for photo-disruptive induced therapy. The laser  
 95 system has been implemented into the modular nonlinear microscopy setup, allowing near-IR two-  
 96 photon excitation and fast detection for FLIO.



97  
 98 *Fig. 1. Laser parameter space. The part of the parameter space of the standard 2PE imaging lasers is denoted*  
 99 *with orange line and shade. The data from the literature on laser sources used in photocoagulation therapy*  
 100 *[19,21,25–31] is denoted with black dots emphasized inside the grey shaded area. Blue lines and shades denote*  
 101 *the part of the parameter space covered by the master-oscillator power-amplifier gain-switched fiber laser, with*  
 102 *an additional area reached by burst mode operation.*

## 103 2 Experimental setups

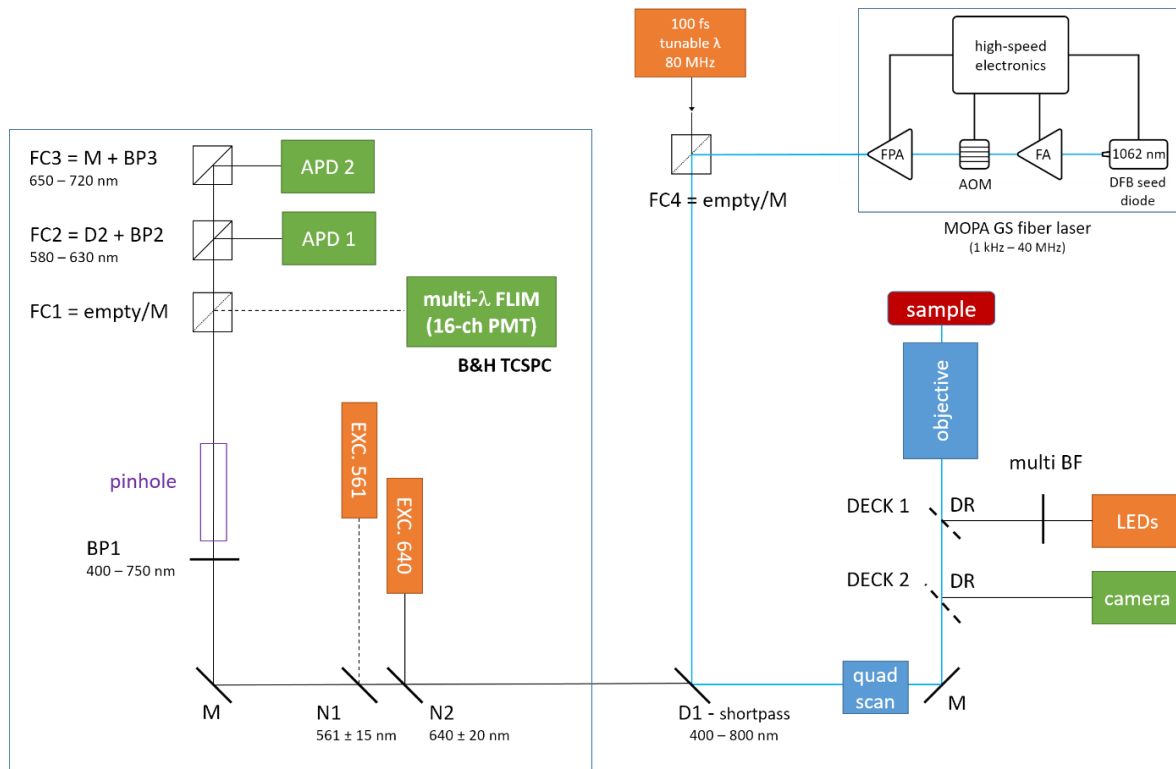
### 104 2.1 Laser source

105 The master-oscillator power-amplifier (MOPA) gain-switched (GS) fiber laser source, shown in top the  
 106 right corner of Fig. 2, is a compact all-fiber MOPA where a gain-switched distributed-feedback (DFB)  
 107 laser diode ( $\lambda = 1062$  nm) is used to generate laser pulses as short as 65 ps at up to 40 MHz repetition  
 108 rate [32]. Key parts of the laser system are seed source and especially its driver and fiber-coupled AOM.  
 109 Seed source driver is capable of generating sub ns electrical pulses with high amplitude (over 50 V) at  
 110 a high repetition rate. These two parameters (pulse duration and amplitude) are the key in order to  
 111 achieve a short optical pulse duration (down to 65 ps) while driving standard DFB laser diode. To reach  
 112 relatively high optical pulse energy it is required to maintain adequate signal to noise (S/N) ratio of the  
 113 optical signal in the laser amplifiers chain at a low repetition rate. Another key component is a high-  
 114 speed electronic circuit that precisely synchronizes and controls both seed driver and AOM as well as  
 115 the laser pump system. As a result, the laser repetition rate can be set in a broad range from 40 MHz  
 116 to 1 kHz [33] and the output pulse energy can be set from a few nJ to approximately 15  $\mu$ J  
 117 independently of the repetition rate. The concept allows the laser to operate in a burst mode that  
 118 includes compensation of the saturation effect appearing in the amplifier chain. Consequently, the  
 119 energy of almost every individual pulse can be set independently within a certain time slot. Therefore,  
 120 the high flexibility and beam quality of this laser enable the use of the same laser for diagnostics as  
 121 well as for therapeutics. While laser systems with equal or even better properties exist, such as Spirit  
 122 by Spectra-Physics or Pharos by Light Conversion, the complexity of those sources manifests in a higher  
 123 up-front price and lower reliability compared to the MOPA fiber laser prototype.

### 124 2.2 Multi-photon imaging system

125 A multi-photon multimodal laser-scanning imaging system (Abberior Instruments) was used for *ex-vivo*  
126 studies of human retinal tissue (see the schematic on Fig. 2). The compact imaging system is composed  
127 of more fluorescence excitation units: one-photon excitation (100 ps pulsed lasers at 561 nm and  
128 640 nm with repetition rate up to 80 MHz and a max output of 200  $\mu$ W) and two-photon excitation  
129 (MOPA GS fiber laser with 65 ps pulse length at 1062 nm with tuneable repetition rate 1 kHz - 40 MHz  
130 and maximum output power of up to 15 W). Additional femtosecond Ti:Sapphire laser (Chameleon,  
131 Coherent) was installed for complementary experiments of two-photon excitation. Various photon  
132 counter detectors were used to detect the fluorescence: two avalanche photodiodes (APD, SPCM-  
133 AQRH, Excelitas), each for the individual one-photon excitation laser with the fluorescence recording  
134 within spectral bands 580 – 625 nm and 655 – 720 nm (filters by Semrock), and 16-channel PMT  
135 detectors (PML-16-GaAsP, Hamamatsu) accompanied with a time-correlated single-photon counter  
136 unit (TCSPC-SPC-150, Becker&Hickl) to acquire additional hyperspectral information of fluorescence  
137 decays (tuneable 200 nm range in visible spectra). An additional band-pass filter was mounted to  
138 prevent scattered or reflected light entering the detectors. Experiments were performed using a 10x  
139 and 60x magnification objectives with the numerical apertures of NA = 0.3 and NA = 1.2 (both  
140 Olympus). Images were performed as well with the wide-field illumination using LED source of the  
141 wavelength 400 nm and CCD camera. Images using laser scanning system were obtained by fast galvo  
142 scanning (Quad Scanner, Abberior Instruments) with a pixel dwell time of max. 10  $\mu$ s and with more  
143 accumulations over predefined scan region in case of low sample signal. Total scan time varied from  
144 few seconds to few minutes.

145 Fluorescence lifetime imaging (FLIM) was recorded with TCSPC [34] synchronized with the laser  
146 excitation through fast FPGA communication. The complete fluorescence decay curve was recorded in  
147 each image pixel separately. In order to gain a sufficient number of detected counts and thus good S/N  
148 ratio, pixel binning had to be used. To obtain a good temporal resolution of the fluorescence decay  
149 when low signal counts were detected, we have chosen a conservatively higher binning in order to  
150 preserve reasonable spatial resolution. Typical binning when acquiring an image with 256 x 256 pixels  
151 and with sufficient signal was set to 2, while in the case of low signal a few times more. The curve  
152 fitting using bi-exponential fit was done with software package SPImage (Becker&Hickl). Fitted  
153 parameters were represented with color-coded maps and accompanying histograms. Data is focused  
154 on representing the average fluorescence decay time ( $\tau_m$ ).



155

156 *Fig. 2. Scheme of the optical setup. Laser sources are shown in orange color, detection modules in green color.*  
 157 *Theranostic study on the ex-vivo human retina was mainly focused on using two-photon ps laser source with*  
 158 *tunable repetition rate (MOPA GS fiber laser) and multi-channel PMT detector with time-correlated single-photon*  
 159 *counter (B&H). D – dichroic; DR – dichroic removable; FC – filter cube; M – mirror; BP – bandpass filter; N – notch*  
 160 *filter.*

161 **2.3 Sample preparation**

162 Theranostics studies were performed on ex-vivo human retinal tissue. Samples were taken from the  
 163 enucleated eyes of the patients with severe illness in compliance with national legislation and with the  
 164 written approval of the patients. Surgical scissors and razor blade were used to separate anterior from  
 165 the posterior eye segment. The posterior part of an eye excluding vitreous was placed into formalin  
 166 fixative for 2 hours at the room temperature and preserved at 4 °C prior measurements.

167

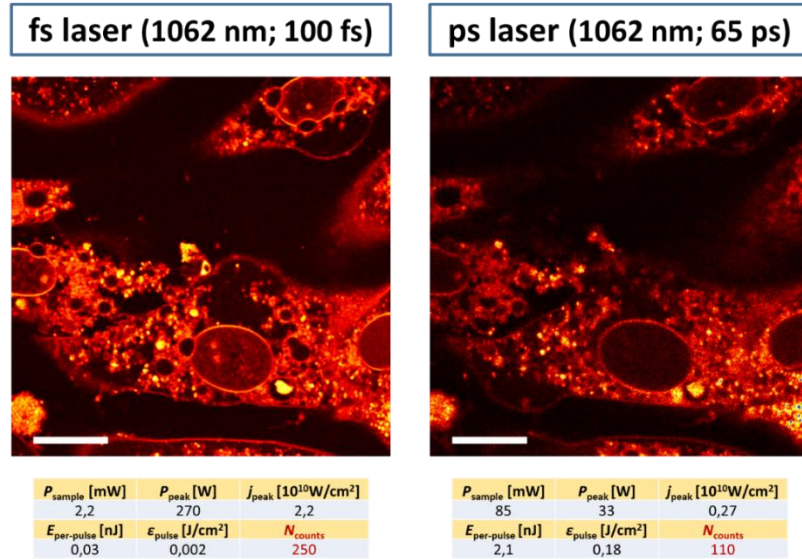
168 **3 Results**

169 **3.1 Quantification of two-photon excitation capability of MOPA GS fiber laser**

170 To quantify the ability for two-photon excitation to perform diagnostics, a comparison was done with  
 171 the standard two-photon excitation source (mode-locked Ti:Sapphire laser; Chameleon, Coherent)  
 172 (Fig. 3, left) using the same near-IR excitation wavelength 1062 nm. The study was performed on the  
 173 biological sample of the *in-vitro* epithelium model composed of epithelial cell line LA4 labelled with  
 174 rhodamine B based membrane probe with good two-photon absorption cross-section.

175 In brief, two-photon excitation is strongly dependent on the peak photon density or photon flux that  
 176 can be in principal reached by the ultrashort fs to ps laser pulses. Since the electron excitation from  
 177 the ground to the first excited state is done via an intermediate, very short-lived forbidden energy  
 178 state, the same molecule must absorb two photons in virtually no time, which demands high photon  
 179 flux. Based on the generally accepted perception, pulse durations of few tens of ps, typical for our

180 MOPA GS fiber laser, would be considered insufficient for the non-linear two-photon excitation.  
 181 However, it can be seen from Fig. 3, that MOPA GS fiber laser (set at a 40 MHz repetition rate) can  
 182 effectively excite fluorescent molecules by two-photon excitation despite an approximately 10-times  
 183 lower peak photon density ( $j$ ) compared to the classical mode-locked fs laser ( $t = 100$  fs,  $\nu = 80$  MHz).  
 184 The threshold intensity for two-photon excitation for MOPA GS fiber laser (assuming on 1% of photons  
 185 detected;  $N_{\text{counts}}/N_{\text{pulses}}$ ) was estimated to be approximately  $j = 5 \cdot 10^8$  W/cm<sup>2</sup>. The comparison of the  
 186 experimental parameters between implemented laser systems is shown in the bottom.



187  
 188 Fig. 3. Quantitative comparison of two-photon excitation using standard fs and MOPA ps pulsed laser on epithelial  
 189 cells in-vitro model labelled with 200  $\mu$ l 10<sup>-5</sup> M rhodamine based membrane probe. Image size is 500\*500 pixels  
 190 with pixel dwell time of 10  $\mu$ s. Focal plane moved slightly between the two acquisitions measurements. Scale bar  
 191 is 10  $\mu$ m.

192  
 193 3.2 Quantification of two-photon diagnostics of MOPA GS fiber laser on ex-vivo retinal tissue

194 Since MOPA GS fiber laser was found appropriate for two-photon excitation, we have then tested its  
 195 applicability on the relevant sample of ex-vivo retinal tissue. Besides performing conventional FAF, we  
 196 have tested the capability of fluorescence lifetime imaging which can provide besides morphological  
 197 also functional information, essential for any diagnostics.

198 FLIM analysis was done by fitting the fluorescence decay curve  $f_m(t)$  with the convolution integral  
 199 between the instrument response function (IRF) and the double-exponential decay model  $f(t)$ :

200 
$$f_m(t) = \int_{\tau=0}^t f(t)IRF(t - \tau) d\tau$$

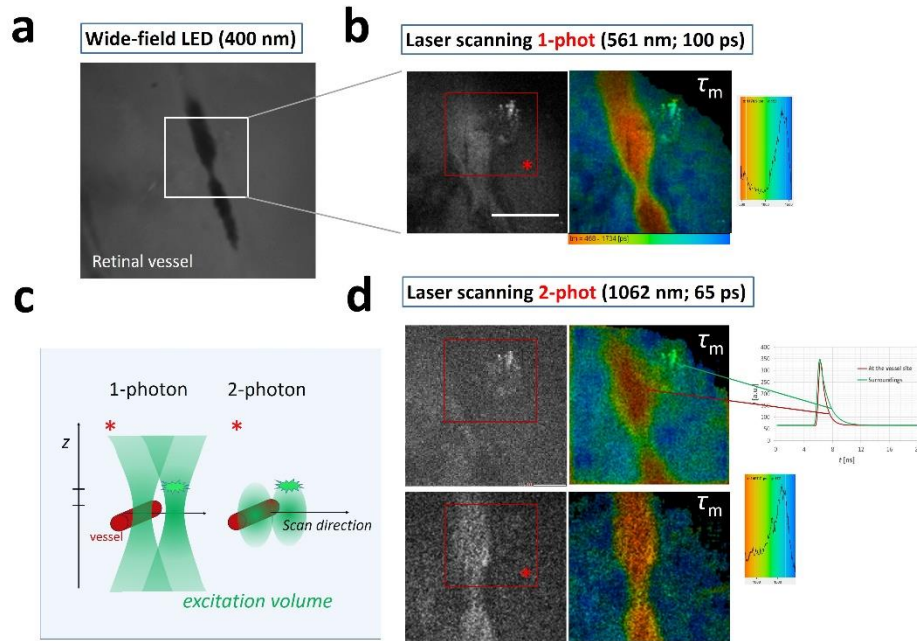
201 
$$f(t) = a_1Exp(-t/\tau_1) + a_2Exp(-t/\tau_2)$$

202 Relative amplitudes ( $a_1$  and  $a_2$ ) and the lifetimes ( $\tau_1$  and  $\tau_2$ ) of the exponential decay were used to  
 203 calculate the descriptive mean lifetime  $\tau_m$  as:

204 
$$\tau_m = \frac{a_1\tau_1 + a_2\tau_2}{a_1 + a_2}$$

205 As shown in Fig. 4,  $\tau_m$  decreases significantly at the vessel site, measured both with one-photon as well  
 206 as two-photon excitation using MOPA GS fiber laser. The corresponding fits of the decay curves on

207 vessel site and surrounding neural retinal tissue are shown in the inset of the Fig. 4d.  $\tau_m$  at vessel site  
 208 was measured  $500 \pm 50$  ps while in the surrounding neural retinal tissue  $1400 \pm 100$  ps. From the  
 209 images, one can also see that the  $\tau_m$  varies across the blood vessel enabling detection of the vessel  
 210 morphology. Finally, the results nicely show the comparison of the resolution and the sensitivity  
 211 between one-photon and two-photon excitation.



212  
 213 *Fig. 4. Comparison of fluorescence lifetime imaging using one-photon and two-photon laser excitation. Better*  
 214 *axial resolution was acquired using two-photon MOPA GS fiber laser with a few times lower S/N ratio. a) The*  
 215 *vessel of a fixed ex-vivo human retina imaged with wide-field LED illumination. b) The same region imaged with*  
 216 *one-photon (labelled 1-phot) laser scanning showing fluorescence lifetime using PMT detector and TCSPC unit*  
 217 *(B&H). c) Schematics of excitation volumes of one-photon and two-photon laser sources. d) Two-photon*  
 218 *fluorescence lifetime (labelled 2-phot) imaged at different axial planes using MOPA GS fiber laser. The*  
 219 *fluorescence lifetime was fitted with two components,  $\tau_m$  representing the mean lifetime. Laser parameters were*  
 220  *$P_{avg} = 50 \mu W$  with 50 MHz repetition rate for one-photon and  $P_{avg} = 400 mW$  with 40 MHz repetition rate for two-*  
 221 *photon. The image resolution is  $128 \times 128$  with  $2 \mu m/pixel$ . Scale bar is  $100 \mu m$ .*

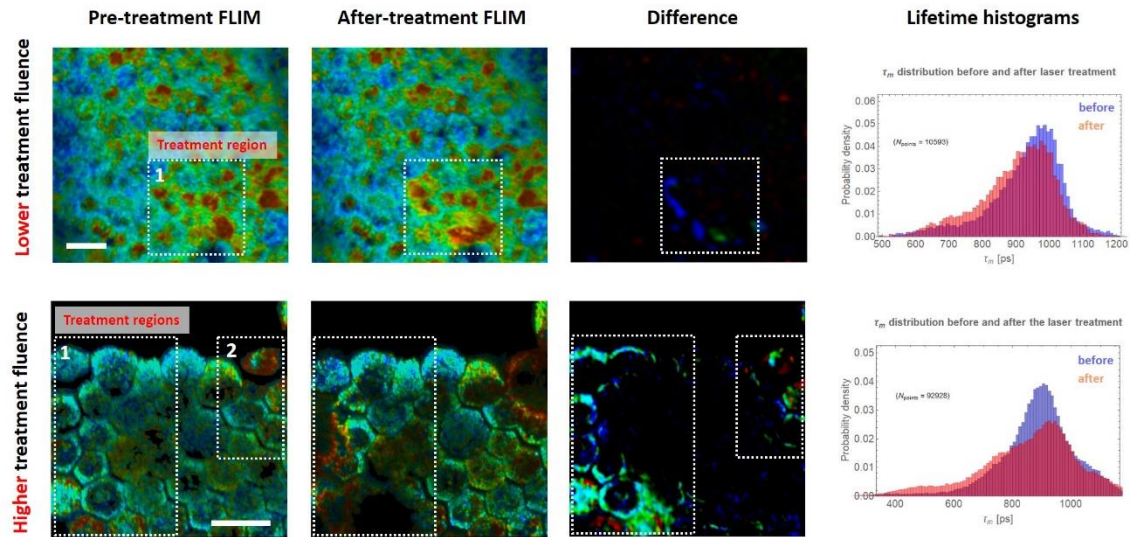
222  
 223 **3.3 Quantification of two-photon diagnostics and therapy of MOPA GS fiber laser on ex-vivo retinal**  
 224 **tissue**

225 Next, MOPA GS fiber laser has been employed to do subsequent diagnostics and therapy on the same  
 226 sample site. Theranostics was performed on the retinal epithelial layer (RPE) on two different sites (Fig.  
 227 5) with different therapy settings. FLIM based pre-diagnostics was followed by an adaptive low-  
 228 frequency operation therapeutic laser targeted to the regions shown within white dotted rectangles.  
 229 By pre-diagnostics, local regions with lower measured  $\tau_m$  have been attributed to higher local melanin  
 230 content (marked with red color) since it is well known that melanin has up to 50% shorter lifetime than  
 231 surrounding lipofuscin [35]. To perform the therapy, pulse fluence was selected to induce first a  
 232 noticeable and second, a significant local structural damage (Fig. 5, lower experiment). 40-times higher  
 233 fluence was needed in comparison to diagnostics pulses, that is  $0.5 J/cm^2$  for first experiment and  
 234  $1 J/cm^2$  for the second. The corresponding pulse energies were  $0.1 \mu J$  and  $0.2 \mu J$ . By post-diagnostics  
 235 analysis, areas that were affected by the therapeutic pulses inside the therapy region have changed  
 236 structurally as well as functionally shown by FLIM analysis. The difference is more pronounced in the  
 237 experiment shown in the bottom (Fig. 5, 3rd column). The main changes are seen through the local



238 shifts in  $\tau_m$ , presented in histograms (Fig. 5, 4th column) and through the partial disappearance of the  
 239 RPE region, the effect known for a successful selective retinal therapy (SRT) that can be a consequence  
 240 of either the cell death [36] or the local laser ablation [37].

241



242

243 *Fig. 5. Diagnostics and therapy of targeted fixed human RPE using the same MOPA GS fiber two-photon laser*  
 244 *using low and high magnification objectives. The regions of laser treatment are denoted with white rectangles.*  
 245 *The pre- and post-diagnostics was analyzed by calculating  $\tau_m$ . Sites affected by treatment pulses) are clearly*  
 246 *visible as seen on the presented difference. The average laser power was the same for diagnostics and treatment*  
 247 *( $P_{avg} \approx 100mW$  and  $P_{avg} \approx 200mW$ ), while the fluence and the energy per pulse were 40-times higher for the*  
 248 *treatment ( $\epsilon_{pulse} \approx 0.5 J/cm^2$ ;  $E_{pulse} \approx 0.1 \mu J$  and  $\epsilon_{pulse} \approx 1 J/cm^2$ ;  $E_{pulse} \approx 0.2 \mu J$ ). The total treatment time at each*  
 249 *region was 30 s. The total diagnostics time was 100 s. Scale bar is  $20 \mu m$ .*

250

#### 251 4 Discussion

252 The results presented in Fig. 4 nicely show the comparison of two-photon MOPA GS fiber laser with  
 253 the one-photon diode laser regarding the resolution and the sensitivity. MOPA GS fiber laser can  
 254 achieve almost the same spatial resolution of the fluorescence lifetime  $\tau_m$  compared to one-photon  
 255 excitation (see the vessel region on Fig. 4b and d). However, significantly higher S/N ratio was acquired  
 256 using one-photon excitation, originating in a much higher photon absorption probability, compared to  
 257 the two-photon nonlinear process [38]. Thus, the energy of the two-photon laser necessary to acquire  
 258 relevant FLIM images with the similar sensitivity of retinal vessels was relatively high, but still below  
 259 the threshold for altering the tissue or the therapeutic effect.

260 On the other hand, two-photon laser enabled the detection of the retinal structures at higher depths  
 261 and with better axial resolution (see the marked red region). We could locate the vessel and the nearby  
 262 pathology clearly at different axial planes, not observed with the one-photon laser, where both  
 263 structures seem to be in the same axial plane (Fig. 4b and d). This is attributed to more localized  
 264 excitation volume schematically represented in Fig. 4c.

265 With both lasers,  $\tau_m$  at vessel site was measured  $500 \pm 50$  ps while in the surrounding neural retinal  
 266 tissue  $1400 \pm 100$  ps. Low  $\tau_m$  at the vessel site is mainly due to hemoglobin presence which contributes  
 267 to short fluorescence decay component  $\tau_1$ , calculated  $270 \pm 30$  ps, which is in a good agreement with  
 268 the results published recently [39]. Measured lifetime components in the surrounding neural retinal  
 269 tissue,  $\tau_1 = 600 \pm 100$  ps and  $\tau_2 = 2500 \pm 300$  ps, on the other hand partially match with the ones in the

270 published data [35].  $\tau_2$  agrees very nicely with the known lifetimes of the most abundant endogenous  
271 molecules, such as FAD, collagen, and lipofuscin, while  $\tau_1$  was measured longer compared to the  
272 literature. This could be attributed to changes in the intrinsic fluorescence properties due to chemical  
273 fixation that can cause an increase in fluorescence lifetime [40,41]. However, the fixation of the tissues  
274 preserves metabolic contrast, the relationship of the lifetimes, and thus the functional information.

275 The presented applicability of the adaptive MOPA GS fiber laser for retinal diagnostics was further  
276 tested for potential applicability in retinal therapy. The results are summarized in Fig. 5, where pre-  
277 diagnostics, therapy and post-diagnostics using different modalities of the laser were done on retinal  
278 RPE on two different sites with different laser treatment settings. The therapeutic laser parameters  
279 were set in such a way to create noticeable (first experiment) to significant structural damage (second  
280 experiment). A 40-times higher fluence compared to the diagnostic pulse was needed to induce  
281 damage, which was achieved by lowering the laser frequency to 1 MHz. The effect of the increased  
282 energy per pulse was observed locally within the chosen treatment region on the few sites with the  
283 higher average melanin content than in surroundings. .

284 The local change in  $\tau_m$  shows that the effect is highly dependent on the local molecular environment,  
285 rich in waste material (lipofuscin) and essentially, absorbing melanin specific for retinal pigment  
286 epithelium. Furthermore, the effect causes local reduction of the autofluorescence signal as well, that  
287 was particularly shown for short therapy laser pulses before [36]. Due to the orders of magnitude  
288 shorter laser pulses that deliver lower energy doses, a negligible thermal effect was induced as  
289 opposed to the known thermal photocoagulation therapies [42]. High peak powers reaching  $10^{11}$   
290 W/cm<sup>2</sup> irradiance rather introduced local plasma mediated ablation [43] on the sites with high melanin  
291 content. Melanin can thus indirectly or directly contribute to the changes in fluorescence lifetime –  
292 the effect, which has already been documented [44]. It is almost surprising to note, that melanin, a  
293 complex mixture of different biopolymers derived from tyrosine, known as a broadband absorber, can  
294 even express a complex emission decay with fluorescence decay ranging from ps to ns [17]. Another  
295 explanation for the decrease in the lifetime in those local regions would be a photo-disruptive effect  
296 of laser on lipofuscin rich molecules with longer lifetimes that lose part of the fluorescence.

297 We have shown that both functional diagnostics using FLIM and local therapy inducing photo-ablation  
298 can be done by the same laser source. However, the study was performed on the fixated *ex-vivo* retina  
299 thus questioning the relevance of the used theranostics parameters for *in-vivo*. It was previously shown  
300 that fixation can cause a change in the scattering coefficient and retardance to the tissue but the  
301 absorption coefficient remains unchanged [45]. We can thus expect that therapeutic parameters  
302 would not be significantly changed when targeting non-fixated tissues.

303 To sum up, the developed MOPA GS fiber laser has fulfilled several demands for the technology being  
304 applicable in future theranostics:

305 1) Capability of operating at a high repetition rate and sufficient fluence (orange shade of parameter  
306 space in Fig. 1) in a controlled, scanning-like approach [46] to collect diagnostics signal in order to  
307 localize the following therapeutic pulses (Fig. 4 and Fig. 5);

308 2) Energy per pulse as well as repetition rate were adaptable depending on the mode of action.  
309 Diagnostics mode used low power and high repetition rate (orange shade of parameter space in  
310 Fig. 1) and in therapy mode vice versa (blue shades of parameter space in Fig. 1);

311 3) By merging the two modes of action – diagnostics and therapy, the system reduces the need of  
312 more sophisticated eye-tracking systems;

313 4) The system is cost-effective, which is beneficial once introduced into clinics.

314

315 **5 Conclusions**

316 Compact fiber-laser-based on high-speed gain-switched DFB laser diode has been shown to achieve  
317 adaptable / independently tuneable repetition rate and energy per pulse allowing coupled two-photon  
318 fluorescence lifetime diagnostics and photo-induced ablation therapy of local molecular environment  
319 in a complex retinal tissue. Several demands for potential applicability in future theranostics were met  
320 and discussed thoroughly. This was the first example of implementing a cost-effective adaptive laser  
321 source to show efficient simultaneous two-photon based functional diagnostics and therapy on the  
322 relevant human *ex-vivo* retinal sample. However, further laser development is needed before  
323 application in clinical trials that could eventually enable advanced theranostics of retinal tissues *in-*  
324 *vivo*.

325

326 **Acknowledgements**

327 The work was primarily carried out in the framework of the GOSTOP program, which is partially  
328 financed by the Republic of Slovenia – Ministry of Education, Science and Sport, and the European  
329 Union – European Regional Development Fund, as well as in the framework of L7-7561 project, which  
330 is financed by the Slovenian Research Agency ARRS. In addition, this work was also partially supported  
331 by other projects of the Slovenian Research Agency ARRS (L2-8183, L2-6780, P2-0270, P2-0392, P1-  
332 0060). We would like to acknowledge also the group of prof. B. Drnovšek Olup on the Department of  
333 Ophthalmology of the University Medical Clinical Centre Ljubljana to provide us the access to the ex-  
334 vivo samples of the retinal tissue.

335

336 **References**

- 337 [1] F.C. Delori, C.K. Dorey, G. Staurenghi, O. Arend, D.G. Goger, J.J. Weiter, In vivo fluorescence of  
338 the ocular fundus exhibits retinal pigment epithelium lipofuscin characteristics, Invest.  
339 Ophthalmol. Vis. Sci. 36 (1995) 718–729.
- 340 [2] A. von Rückmann, F.W. Fitzke, A.C. Bird, Distribution of fundus autofluorescence with a scanning  
341 laser ophthalmoscope, Br J Ophthalmol. 79 (1995) 407–412.  
342 <https://doi.org/10.1136/bjo.79.5.407>.
- 343 [3] A.F. Fercher, K. Mengedoht, W. Werner, Eye-length measurement by interferometry with  
344 partially coherent light, Opt. Lett., OL. 13 (1988) 186–188.  
345 <https://doi.org/10.1364/OL.13.000186>.
- 346 [4] W. Drexler, U. Morgner, R.K. Ghanta, F.X. Kärtner, J.S. Schuman, J.G. Fujimoto, Ultrahigh-  
347 resolution ophthalmic optical coherence tomography, Nature Medicine. 7 (2001) 502–507.  
348 <https://doi.org/10.1038/86589>.
- 349 [5] J. Marshall, The ageing retina: Physiology or pathology, Eye. 1 (1987) 282–295.  
350 <https://doi.org/10.1038/eye.1987.47>.
- 351 [6] J. Sparrow, T. Duncker, J.R. Sparrow, T. Duncker, Fundus Autofluorescence and RPE Lipofuscin in  
352 Age-Related Macular Degeneration, Journal of Clinical Medicine. 3 (2014) 1302–1321.  
353 <https://doi.org/10.3390/jcm3041302>.
- 354 [7] J. Teister, A. Liu, D. Wolters, N. Pfeiffer, F.H. Grus, Peripapillary fluorescence lifetime reveals age-  
355 dependent changes using fluorescence lifetime imaging ophthalmoscopy in rats, Experimental  
356 Eye Research. 176 (2018) 110–120. <https://doi.org/10.1016/j.exer.2018.07.008>.

- 357 [8] J. Schmidt, S. Peters, L. Sauer, D. Schweitzer, M. Klemm, R. Augsten, N. Müller, M. Hammer,  
358 Fundus autofluorescence lifetimes are increased in non-proliferative diabetic retinopathy, *Acta*  
359 *Ophthalmologica*. 95 (2017) 33–40. <https://doi.org/10.1111/aos.13174>.
- 360 [9] L. Sauer, R.H. Gensure, M. Hammer, P.S. Bernstein, Fluorescence Lifetime Imaging  
361 Ophthalmoscopy: A Novel Way to Assess Macular Telangiectasia Type 2, *Oph Retina*. 2 (2018)  
362 587–598. <https://doi.org/10.1016/j.oret.2017.10.008>.
- 363 [10] D. Schweitzer, L. Deutsch, M. Klemm, S. Jentsch, M. Hammer, S. Peters, J. Haueisen, U.A. Müller,  
364 J. Dawczynski, Fluorescence lifetime imaging ophthalmoscopy in type 2 diabetic patients who  
365 have no signs of diabetic retinopathy, *JBO, JBOPFO*. 20 (2015) 061106.  
366 <https://doi.org/10.1117/1.JBO.20.6.061106>.
- 367 [11] J.A. Feeks, J.J. Hunter, Adaptive optics two-photon excited fluorescence lifetime imaging  
368 ophthalmoscopy of exogenous fluorophores in mice, *Biomed. Opt. Express*, BOE. 8 (2017) 2483–  
369 2495. <https://doi.org/10.1364/BOE.8.002483>.
- 370 [12] C. Dysli, R. Fink, S. Wolf, M.S. Zinkernagel, Fluorescence Lifetimes of Drusen in Age-Related  
371 Macular Degeneration, *Invest. Ophthalmol. Vis. Sci*. 58 (2017) 4856–4862.  
372 <https://doi.org/10.1167/iovs.17-22184>.
- 373 [13] L. Sauer, C.B. Komanski, A.S. Vitale, E.D. Hansen, P.S. Bernstein, Fluorescence Lifetime Imaging  
374 Ophthalmoscopy (FLIO) in Eyes With Pigment Epithelial Detachments Due to Age-Related  
375 Macular Degeneration, *Invest Ophthalmol Vis Sci*. 60 (2019) 3054–3063.  
376 <https://doi.org/10.1167/iovs.19-26835>.
- 377 [14] D. Schweitzer, S. Schenke, M. Hammer, F. Schweitzer, S. Jentsch, E. Birckner, W. Becker, A.  
378 Bergmann, Towards metabolic mapping of the human retina, *Microscopy Research and*  
379 *Technique*. 70 (2007) 410–419. <https://doi.org/10.1002/jemt.20427>.
- 380 [15] C. Dysli, S. Wolf, M.Y. Berezin, L. Sauer, M. Hammer, M.S. Zinkernagel, Fluorescence lifetime  
381 imaging ophthalmoscopy, *Progress in Retinal and Eye Research*. 60 (2017) 120–143.  
382 <https://doi.org/10.1016/j.preteyeres.2017.06.005>.
- 383 [16] A. Periasamy, P. Wodnicki, X.F. Wang, S. Kwon, G.W. Gordon, B. Herman, Time-resolved  
384 fluorescence lifetime imaging microscopy using a picosecond pulsed tunable dye laser system,  
385 *Review of Scientific Instruments*. 67 (1996) 3722–3731. <https://doi.org/10.1063/1.1147139>.
- 386 [17] A. Ehlers, I. Riemann, M. Stark, K. König, Multiphoton fluorescence lifetime imaging of human  
387 hair, *Microscopy Research and Technique*. 70 (2007) 154–161.  
388 <https://doi.org/10.1002/jemt.20395>.
- 389 [18] B. Leskovar, C.C. Lo, P.R. Hartig, K. Sauer, Photon counting system for subnanosecond  
390 fluorescence lifetime measurements, *Review of Scientific Instruments*. 47 (1976) 1113–1121.  
391 <https://doi.org/10.1063/1.1134827>.
- 392 [19] J. Roider, S.H.M. Liew, C. Klatt, H. Elsner, E. Poerksen, J. Hillenkamp, R. Brinkmann, R. Birngruber,  
393 Selective retina therapy (SRT) for clinically significant diabetic macular edema, *Graefes Arch Clin*  
394 *Exp Ophthalmol*. 248 (2010) 1263–1272. <https://doi.org/10.1007/s00417-010-1356-3>.
- 395 [20] E. Seifert, J. Tode, A. Pielen, D. Theisen-Kunde, C. Framme, J. Roider, Y. Miura, R. Birngruber, R.  
396 Brinkmann, Selective retina therapy: toward an optically controlled automatic dosing, *J Biomed*  
397 *Opt*. 23 (2018) 1–12. <https://doi.org/10.1117/1.JBO.23.11.115002>.

- 398 [21] S. Al-Hussainy, P.M. Dodson, J.M. Gibson, Pain response and follow-up of patients undergoing  
399 panretinal laser photocoagulation with reduced exposure times, *Eye*. 22 (2008) 96–99.  
400 <https://doi.org/10.1038/sj.eye.6703026>.
- 401 [22] S.V. Reddy, D. Husain, Panretinal Photocoagulation: A Review of Complications, *Seminars in*  
402 *Ophthalmology*. 33 (2018) 83–88. <https://doi.org/10.1080/08820538.2017.1353820>.
- 403 [23] R.H. Guymer, Z. Wu, L.A.B. Hodgson, E. Caruso, K.H. Brassington, N. Tindill, K.Z. Aung, M.B.  
404 McGuinness, E.L. Fletcher, F.K. Chen, U. Chakravarthy, J.J. Arnold, W.J. Heriot, S.R. Durkin, J.J.  
405 Lek, C.A. Harper, S.S. Wickremasinghe, S.S. Sandhu, E.K. Baglin, P. Sharangan, S. Braat, C.D. Luu,  
406 Laser Intervention in Early Stages of Age-Related Macular Degeneration Study Group,  
407 Subthreshold Nanosecond Laser Intervention in Age-Related Macular Degeneration: The LEAD  
408 Randomized Controlled Clinical Trial, *Ophthalmology*. 126 (2019) 829–838.  
409 <https://doi.org/10.1016/j.ophtha.2018.09.015>.
- 410 [24] W.R. Calhoun, I.K. Ilev, Effect of therapeutic femtosecond laser pulse energy, repetition rate, and  
411 numerical aperture on laser-induced second and third harmonic generation in corneal tissue,  
412 *Lasers Med Sci*. 30 (2015) 1341–1346. <https://doi.org/10.1007/s10103-015-1726-5>.
- 413 [25] Z. Hu, H. Zhang, A. Mordovanakis, Y.M. Paulus, Q. Liu, X. Wang, X. Yang, High-precision, non-  
414 invasive anti-microvascular approach via concurrent ultrasound and laser irradiation, *Scientific*  
415 *Reports*. 7 (2017) 40243. <https://doi.org/10.1038/srep40243>.
- 416 [26] J.P.M. Wood, O. Shibebe, M. Plunkett, R.J. Casson, G. Chidlow, Retinal Damage Profiles and  
417 Neuronal Effects of Laser Treatment: Comparison of a Conventional Photocoagulator and a  
418 Novel 3-Nanosecond Pulse Laser, *Invest. Ophthalmol. Vis. Sci*. 54 (2013) 2305–2318.  
419 <https://doi.org/10.1167/iovs.12-11203>.
- 420 [27] Y. Takatsuna, S. Yamamoto, Y. Nakamura, T. Tatsumi, M. Arai, Y. Mitamura, Long-term  
421 therapeutic efficacy of the subthreshold micropulse diode laser photocoagulation for diabetic  
422 macular edema, *Jpn J Ophthalmol*. 55 (2011) 365–369. [https://doi.org/10.1007/s10384-011-](https://doi.org/10.1007/s10384-011-0033-3)  
423 [0033-3](https://doi.org/10.1007/s10384-011-0033-3).
- 424 [28] G. Schuele, H. Elsner, C. Framme, J. Roeder, R. Birngruber, R. Brinkmann, Optoacoustic real-time  
425 dosimetry for selective retina treatment, *JBO, JBOPFO*. 10 (2005) 064022.  
426 <https://doi.org/10.1117/1.2136327>.
- 427 [29] Y.M. Paulus, A. Jain, H. Nomoto, C. Sramek, R.F. Gariano, D. Andersen, G. Schuele, L.-S. Leung, T.  
428 Leng, D. Palanker, SELECTIVE RETINAL THERAPY WITH MICROSECOND EXPOSURES USING A  
429 CONTINUOUS LINE SCANNING LASER, *RETINA*. 31 (2011) 380.  
430 <https://doi.org/10.1097/IAE.0b013e3181e76da6>.
- 431 [30] R.R. Anderson, J.A. Parrish, Selective photothermolysis: precise microsurgery by selective  
432 absorption of pulsed radiation, *Science*. 220 (1983) 524–527.  
433 <https://doi.org/10.1126/science.6836297>.
- 434 [31] W.T. Ham, R.C. Williams, H.A. Mueller, D. Guerry, A.M. Clarke, W.J. Geeraets, Effects of Laser  
435 Radiation on the Mammalian Eye\*†, *Transactions of the New York Academy of Sciences*. 28  
436 (1966) 517–526. <https://doi.org/10.1111/j.2164-0947.1966.tb02368.x>.
- 437 [32] J. Petelin, B. Podobnik, R. Petkovšek, Burst shaping in a fiber-amplifier chain seeded by a gain-  
438 switched laser diode, *Appl. Opt., AO*. 54 (2015) 4629–4634.  
439 <https://doi.org/10.1364/AO.54.004629>.

- 440 [33] M. Šajn, J. Petelin, V. Agrež, M. Vidmar, R. Petkovšek, DFB diode seeded low repetition rate fiber  
441 laser system operating in burst mode, *Optics & Laser Technology*. 88 (2017) 99–103.  
442 <https://doi.org/10.1016/j.optlastec.2016.09.006>.
- 443 [34] W. Becker, *Advanced Time-Correlated Single Photon Counting Techniques*, Springer-Verlag,  
444 Berlin Heidelberg, 2005. [//www.springer.com/la/book/9783540260479](http://www.springer.com/la/book/9783540260479) (accessed September 6,  
445 2018).
- 446 [35] D. Schweitzer, S. Schenke, M. Hammer, F. Schweitzer, S. Jentsch, E. Birckner, W. Becker, A.  
447 Bergmann, Towards metabolic mapping of the human retina, *Microsc. Res. Tech.* 70 (2007) 410–  
448 419. <https://doi.org/10.1002/jemt.20427>.
- 449 [36] J.P.M. Wood, M. Plunkett, V. Previn, G. Chidlow, R.J. Casson, Nanosecond pulse lasers for retinal  
450 applications, *Lasers Surg Med.* 43 (2011) 499–510. <https://doi.org/10.1002/lsm.21087>.
- 451 [37] B. Považay, R. Brinkmann, M. Stoller, R. Kessler, Selective Retina Therapy, in: J.F. Bille (Ed.), *High*  
452 *Resolution Imaging in Microscopy and Ophthalmology: New Frontiers in Biomedical Optics*,  
453 Springer International Publishing, Cham, 2019: pp. 237–259. [https://doi.org/10.1007/978-3-030-](https://doi.org/10.1007/978-3-030-16638-0_11)  
454 [16638-0\\_11](https://doi.org/10.1007/978-3-030-16638-0_11).
- 455 [38] W. Denk, J.H. Strickler, W.W. Webb, Two-photon laser scanning fluorescence microscopy,  
456 *Science*. 248 (1990) 73–76. <https://doi.org/10.1126/science.2321027>.
- 457 [39] I. Saytashev, R. Glenn, G.A. Murashova, S. Osseiran, D. Spence, C.L. Evans, M. Dantus,  
458 Multiphoton excited hemoglobin fluorescence and third harmonic generation for non-invasive  
459 microscopy of stored blood, *Biomed Opt Express*. 7 (2016) 3449–3460.  
460 <https://doi.org/10.1364/BOE.7.003449>.
- 461 [40] NAD(P)H fluorescence lifetime measurements in fixed biological tissues. - PubMed - NCBI, (n.d.).  
462 <https://www.ncbi.nlm.nih.gov/pubmed/31553966> (accessed March 17, 2020).
- 463 [41] D. Schweitzer, E.R. Gaillard, J. Dillon, R.F. Mullins, S. Russell, B. Hoffmann, S. Peters, M. Hammer,  
464 C. Biskup, Time-resolved autofluorescence imaging of human donor retina tissue from donors  
465 with significant extramacular drusen, *Invest. Ophthalmol. Vis. Sci.* 53 (2012) 3376–3386.  
466 <https://doi.org/10.1167/iovs.11-8970>.
- 467 [42] B. Považay, R. Brinkmann, M. Stoller, R. Kessler, Selective Retina Therapy, in: J.F. Bille (Ed.), *High*  
468 *Resolution Imaging in Microscopy and Ophthalmology: New Frontiers in Biomedical Optics*,  
469 Springer International Publishing, Cham, 2019: pp. 237–259. [https://doi.org/10.1007/978-3-030-](https://doi.org/10.1007/978-3-030-16638-0_11)  
470 [16638-0\\_11](https://doi.org/10.1007/978-3-030-16638-0_11).
- 471 [43] G. Keiser, *Light-Tissue Interactions*, in: G. Keiser (Ed.), *Biophotonics: Concepts to Applications*,  
472 Springer, Singapore, 2016: pp. 147–196. [https://doi.org/10.1007/978-981-10-0945-7\\_6](https://doi.org/10.1007/978-981-10-0945-7_6).
- 473 [44] E. Dimitrow, I. Riemann, A. Ehlers, M.J. Koehler, J. Norgauer, P. Elsner, K. König, M. Kaatz,  
474 Spectral fluorescence lifetime detection and selective melanin imaging by multiphoton laser  
475 tomography for melanoma diagnosis, *Experimental Dermatology*. 18 (2009) 509–515.  
476 <https://doi.org/10.1111/j.1600-0625.2008.00815.x>.
- 477 [45] M.F.G. Wood, N. Vurgun, M.A. Wallenburg, I.A. Vitkin, Effects of formalin fixation on tissue  
478 optical polarization properties, *Phys. Med. Biol.* 56 (2011) N115–N122.  
479 <https://doi.org/10.1088/0031-9155/56/8/N01>.

480 [46] M.A. Mainster, G.T. Timberlake, R.H. Webb, G.W. Hughes, Scanning laser ophthalmoscopy.  
481 Clinical applications, *Ophthalmology*. 89 (1982) 852–857. <https://doi.org/10.1016/s0161->  
482 6420(82)34714-4.

483